Simulations of liquid nanocylinder breakup with dissipative particle dynamics

A. Tiwari, H. Reddy, S. Mukhopadhyay, and J. Abraham
School of Mechanical Engineering, Purdue University, West Lafayette, Indiana 47907, USA
(Received 7 February 2008; published 15 July 2008)

In this work, we use a dissipative-particle-dynamics-based model for two-phase flows to simulate the breakup of liquid nanocylinders. Rayleigh's criterion for capillary breakup of inviscid liquid cylinders is shown to apply for the cases considered, in agreement with prior molecular dynamics (MD) simulations. Also, as shown previously through MD simulations, satellite drops are not observed, because of the dominant role played by thermal fluctuations which lead to a symmetric breakup of the neck joining the two main drops. The parameters varied in this study are the domain size, cylinder radius, thermal length scale, viscosity, and surface tension. The breakup time does not show the same scaling dependence as in capillary breakup of liquid cylinders at the macroscale. The time variation of the radius at the point of breakup agrees with prior theoretical predictions from expressions derived with the assumption that thermal fluctuations lead to breakup.

DOI: 10.1103/PhysRevE.78.016305 PACS number(s): 47.61.−k, 47.20.Ma, 02.70.Ns, 47.61.Jd

I. INTRODUCTION

The formation of drops from the breakup of liquid jets at the nanoscale occurs in several applications, including nanoscale machining [1], superfine ink-jet printing [2], lipid bilayer membranes encountered in the Golgi apparatus [3], self-organizing supramolecular cylinders [4], and drug or gene delivery to biological cells [5]. While the formation of drops from the breakup of liquid films and jets at the macroscale has been extensively studied in the literature [6], that of drops at the nanoscale has only recently been investigated, primarily through molecular dynamics (MD) simulations. The behavior of fluids at the macroscopic level is well characterized by equations for Newtonian and non-Newtonian flows, but at the nanolevel physical processes like thermal fluctuations begin to play a significant role in determining the behavior. The standard formulation of the Navier-Stokes equations does not have the capability to reproduce these processes, though progress has been made recently toward developing new formulations [7,8].

Molecular dynamics [9,10] is an obvious choice as a computational tool for the analysis of nanoscale systems. It has been employed for studying the behavior of polymer nanodroplets [11], nanojets [7,12,13], boundary conditions at solid-liquid [14] and liquid-liquid interfaces [15], and mixing process at the nanoscale [16]; but MD is computationally expensive. In fact, the physical size of the systems considered in these studies is at most 50 nm for the large-scale MD computations by Kadau *et al.* [16], using about 100×10^6 particles. Hence, extension of MD to study problems with multiple scales is challenging, unless it is combined with other methods in the framework of multiscale models. To overcome this limitation and at the same time capture essential physics at the submicrometer scales, one approach is to carry out coarse graining at the molecular level. Coarse graining will reduce the hard-core nature of the interaction potential employed in MD, and can reduce the number of particles and increase the size of numerical time steps. Coarse graining, however, is a challenging task because of the need to recalibrate models for the interaction potential, introduce additional models to account for lost degrees of freedom, and calibrate the constants of these models in a self-consistent way [17,18]. In this paper, the capability of a recently developed coarse-grained particle-based method, dissipative particle dynamics (DPD) [19,20], to capture the physics of liquid nanocylinder breakup is assessed. It is worth noting that other methods have been suggested as possible candidates for simulations at the mesolevel. The lattice-Boltzmann method (LBM) [21–24] is one such method. In the case of the LBM, however, the connections to submicrometer-scale physics are not apparent.

The fundamental idea in DPD is to use particles which are conceptually clusters of many actual atoms or molecules. The precise correspondence between the numbers of DPD and MD particles is not generally known *a priori*; hence, a physical length scale is not specified. Alternatively, a physical length scale can be specified *a priori*, and the correspondence between one DPD particle and the number of atoms or molecules employed in MD calculated. It is worth pointing out that systematic methods for coarse graining, where the relationship between physical scales is known, have recently been proposed [17]. Of course, in DPD the molecular details cannot be captured, but Eggers [25] has shown that information at this level is not needed to draw useful conclusions, because the lubrication equation with a stochastic term added, i.e., without molecular details, can reproduce physics that leads to nanocylinder breakup. DPD has been employed for simulating the flow of complex fluids like colloids and biological matter [18,26–28]. More recently, DPD models have also been developed to simulate two-phase flows [29–32]. The two-phase model employed in this work will be discussed later.

Breakup simulations of nanocylinders have been performed by several authors in the past using MD. Koplik and Banavar [33] carried out simulations of the rupture of liquid nanothreads as part of their study of liquid interfaces. They found that the rupture time of liquid nanothreads was of the same order as the analytical time scale for rupture that can be obtained from Rayleigh's classical solution for inviscid liquid cylinders [34]. This solution is based on the criterion that capillary instability causes breakup. It leads to the conclusion that breakup occurs when a disturbance has a wavelength greater than the circumference of the cylinder. It can be

shown that, when this is the case, the surface area of the drop formed is decreased relative to the area of the corresponding cylinder. More recently, Min and Wong [35] arrived at the same conclusion, using their MD simulations of nanothreads. Kawano [36] also performed MD simulations of liquid nanothreads and found a good qualitative match of simulated wavelengths with analytical results from classical linear instability theory. While there are these similarities between nanoscale breakup characteristics and results from classical theories developed to explain macroscale breakup, differences also exist.

Satellite drops are rarely formed at the nanoscale. Rayleigh's inviscid solution does not predict the formation of these drops; but they are predicted through nonlinear analytical formulations and numerical simulations, and observed in experiments [24,37,38]. The satellite drops are formed from the thin ligaments which connect the larger drops during the breakup process. As the wavelength of the disturbance decreases, the ligament becomes shorter and the satellite drop size decreases. That breakup of nanothreads generally does not lead to the formation of satellite drops appears evident in the results of Koplik and Banavar [33], and has been explicitly pointed out by Min and Wong [35]. This conclusion has also been drawn from investigations of the breakup of nanojets, where the breakup occurs through mechanisms similar to those of nanocylinders. Breakup simulations of nanojets by Moseler and Landman [7] employing MD and Tiwari and Abraham [39] employing DPD have also shown the absence of satellite drops. Eggers [25] arrived at the same conclusion by solving a stochastic differential equation derived by Moseler and Landman, in which they added a stochastic term to the lubrication equation describing the evolution of the jet. Eggers has suggested that there may be exceptions where large thermal fluctuations in the symmetric neck may lead to satellite drops.

The absence of satellite drops is attributed to the mechanism of breakup. At the nanoscale, breakup takes place in a symmetric fashion with the presence of double-cone structures that are a signature of the important role played by thermal fluctuations. In other words, the long thin ligaments seen at the macroscale are not observed. There is, however, recent evidence that this is pressure dependent. Kang and Landman [40] carried out MD simulations to determine the shapes of the pinch-off region during breakup of nanocylinders. They concluded that the shape had a symmetric double-cone structure in vacuum, but asymmetric threadlike shapes developed at higher pressures. Whether these then lead to the formation of satellite drops would be interesting to explore. They also found that the solution of the stochastic lubrication equation captured the crossover between the two modes.

Eggers [25] has also studied the dynamics of breakup in detail. He has pointed out an important difference in the evolution of the radius at the breakup location. Macroscopic theory predicts the following relationship for minimum cylinder radius $r_{\min}$ [41,42]:

$$r_{\min} = r_0(T - t), \tag{1}$$

where r_0 is a constant, T denotes the breakup time, and t the current time. When thermal fluctuations play a dominant role, they tend to accelerate the breakup process. Eggers has shown that the following relationship then holds for the minimum radius $r_{\min}$:

$$r_{\min} = r_1(T - t)^{0.418}, \tag{2}$$

where r_1 is a constant and other symbols have the same meaning as in Eq. (1).

In this work, the ability of a DPD two-phase model for liquid-vapor systems to simulate the breakup of liquid nanocylinders is assessed. Similar to the observations made from MD simulations reported in the literature, it is shown that simulated breakup events occur when Rayleigh's criterion is met. Prior work on breakup time of nanocylinders has explored its dependence on the radius of the cylinder and concluded that the scaling relation for breakup time at the macroscale holds at the nanoscale [38]. It will be shown in this work, however, that the scaling holds only when the variations in radius are considered; but, when viscosity and surface tension are also varied, there are noticeable differences and the breakup time does not follow the scaling behavior at the macroscale. The formation of double-cone structures, prior to breakup, is observed. It is shown that satellite drops are not formed. The dynamics near the breakup point follow the theoretical prediction by Eggers.

This paper is organized as follows. In Sec. II we provide a brief overview of the DPD-based two-phase model used in this work. Section III presents the results and discussion of breakup simulations of liquid nanocylinders. We conclude the paper with summary and conclusions in Sec. IV.

II. THE DPD TWO-PHASE MODEL

In this section, for completeness, a brief overview of the DPD-based two-phase model will be provided. A detailed description of the model can be found in Ref. [32]. The position and velocity of a DPD particle i of unit mass are computed from Newton's laws of motion given by

$$\frac{d\mathbf{r}_i}{dt} = \mathbf{v}_i, \quad \frac{d\mathbf{v}_i}{dt} = \mathbf{f}_i, \tag{3}$$

where $\mathbf{r}_i$, $\mathbf{v}_i$, and $\mathbf{f}_i$ denote the position, velocity, and force vectors, respectively. The force on a particle arises from interparticle interactions. This force has three components. The dissipative force component $\mathbf{F}_{ij}^D$ is responsible for the viscous effects in the DPD system; it acts to reduce the relative velocity between any two particles in an interacting pair. As a result the system temperature will be reduced. The random force $\mathbf{F}_{ij}^R$ is included to account for the lost degrees of freedom incurred because of the coarse-graining process. At the molecular level there are many collisions that take place between the actual atoms or molecules. But, when a group of atoms or molecules is represented by a DPD particle, there is a reduction in the number of collisions. The random force tends to "heat" the DPD system as it supplies energy to the interacting particles. If the two forces are balanced, an isothermal system will result. Espanol and Warren [20], by applying the fluctuation-dissipation theorem, have derived the relations that result in this balance. They showed that the

Gibbs equilibrium distribution function is recovered by the model. The dissipative and random forces are responsible for the hydrodynamic behavior of the DPD system. The third component of the interparticle force of interaction is the conservative force $\mathbf{F}_{ij}^{C}$, which accounts for the configurational energy of the DPD system. It is responsible for the thermodynamic behavior of the DPD system.

The functional forms of the interparticle forces between particles i and j are given by

$$\mathbf{F}_{ij}^{D} = -\gamma\omega^{D}(r_{ij})(\mathbf{e}_{ij}\cdot\mathbf{v}_{ij})\mathbf{e}_{ij},$$

$$\mathbf{F}_{ij}^{R} = \sigma\omega^{R}(r_{ij})\xi_{ij}\mathbf{e}_{ij},$$

$$\mathbf{F}_{ij}^{C} = -\frac{\partial\psi(r_{ij})}{\partial r_{ij}}\mathbf{e}_{ij}. \tag{4}$$

Here, $\mathbf{e}_{ij}$ is a unit vector given by $\mathbf{e}_{ij}=\mathbf{r}_{ij}/|\mathbf{r}_{ij}|$, where $\mathbf{r}_{ij}=\mathbf{r}_i-\mathbf{r}_j$, $\mathbf{v}_{ij}=\mathbf{v}_i-\mathbf{v}_j$, γ is the amplitude of the dissipative force, σ is the amplitude of the random force, ω^D and ω^R are the weight functions for the dissipative and random forces, respectively, and ψ is the free energy per particle. Since DPD is a short-range model, the weight functions are chosen such that their values go to zero beyond the cutoff distance, i.e., each particle interacts only with particles that are within the cutoff distance. The term ξ_{ij} in Eq. (4) is a random variable which has zero mean and unit variance, and is uncorrelated in time. It follows Gaussian statistics and has the following properties:

$$\langle\xi_{ij}(t)\rangle = 0,$$

$$\langle\xi_{ij}(t)\xi_{kl}(t')\rangle = (\delta_{ik}\delta_{jl}+\delta_{il}\delta_{jk})\delta(t-t'). \tag{5}$$

The application of the fluctuation-dissipation theorem to the DPD system gives the following relationship between the amplitudes and the weight functions of the dissipative and random forces [20]:

$$\omega^{D}(r) = [\omega^{R}(r)]^2, \quad \sigma^2 = 2\gamma k_B T. \tag{6}$$

In this work, the following functional form for the weight functions in the expressions for the dissipative and random forces have been chosen:

$$\omega^{D}(r) = [\omega^{R}(r)]^2 = \begin{cases} \left(1-\dfrac{r}{r_c}\right)^2 & (r<r_c), \\ 0 & (r\geq r_c). \end{cases} \tag{7}$$

These weight functions depend on the interparticle separation r and the cutoff radius r_c. Additional details about the force components and the choice of parameters employed in this work can be found in the article by Groot and Warren [43].

The implementation of the interfacial forces will now be described briefly. These forces are molecular in origin, in that the intermolecular forces between liquid-liquid molecules, gas-gas molecules and liquid-gas molecules are different. The differences give rise to phase segregation and the macroscopic property of surface tension. In this work, the mean-field-theory-based model of Tiwari and Abraham [32] is used. The essential idea is to model the force component which influences the interparticle force [44,45]. This approach has been employed successfully in other mesoscopic approaches [23,24,46]. The conservative force $\mathbf{F}^C$ is expressed as

$$\mathbf{F}^{C} = -\boldsymbol{\nabla}\psi_{\text{nonideal}} + \kappa\boldsymbol{\nabla}\nabla^2\rho, \tag{8}$$

where ψ_{nonideal} denotes the nonideal part of the free energy, ρ is the density, and κ is a model parameter that controls the strength of surface tension; it is related to the second moment of the attractive part of the interaction potential between atoms or molecules. In Eq. (8) the first term is responsible for phase segregation and the second for surface tension. The expression for the free energy, required in Eq. (8), is derived from an equation of state with a van der Waals loop. In this work, the following van der Waals equation of state is used:

$$p = \frac{\rho k_B T}{1-b\rho} - a\rho^2, \tag{9}$$

where p denotes the pressure, ρ the density, k_B the Boltzmann constant, and T the temperature, and a and b are parameters of the equation of state which are related to the zeroth moment of the attractive part of the interaction potential and the exclusion volume effects, respectively. It can be seen from Eq. (8) that the surface tension term depends on the gradients of density. The density ρ in the vicinity of particle i is calculated using the following expression:

$$\rho_i = \sum_{j=1}^{N} w(r_{ij}), \tag{10}$$

where w, j, r, and N represent the normalized weight function, a particle tag, the separation distance, and the total number of particles, respectively. Note that the form of weight function used for the dissipative and random forces in Eq. (7) would not suffice for Eq. (10) as the third derivative of density has to be calculated in Eq. (8). Hence, the Lucy weight function is used [47]. It has been employed extensively in other particle-based methods [48,49], and is given by

$$w(r,r_c) = \begin{cases} c\left(1+\dfrac{3r}{r_c}\right)\left(1-\dfrac{r}{r_c}\right)^3 & \text{if } r<r_c, \\ 0 & \text{if } r>r_c, \end{cases} \tag{11}$$

where r denotes the interparticle separation, r_c the cutoff radius, and c the normalization constant, which has a value $5/\pi r_c^2$ for two dimensions and $105/16\pi r_c^3$ for three dimensions. Using the definition of density in Eq. (10) and substituting the free energy obtained from Eq. (9) into Eq. (8), the final form of the interparticle conservative force is obtained as

$$\mathbf{F}_{ij}^{C} = \left\{-\left[\left(\frac{bk_BT}{1-b\rho_i}-a\right)+\left(\frac{bk_BT}{1-b\rho_j}-a\right)\right]w_{ij}^{(1)} + \kappa w_{ij}^{(3)}\right\}\mathbf{e}_{ij}, \tag{12}$$

where $w_{ij}^{(1)}$ and $w_{ij}^{(3)}$ represent the first and third derivatives of the weight function in Eq. (11) with respect to the interpar-

ticle separation, respectively. The parameters that are required for specifying the interparticle conservative force are a, b, κ, r_c, and k_BT.

The DPD equations of motion are integrated using the following modified Verlet scheme by Groot and Warren [43]:

$$\mathbf{r}_i(t+\delta t) = \mathbf{r}_i(t) + \delta t \mathbf{v}_i(t) + \frac{1}{2}(\delta t)^2 \mathbf{f}_i(t),$$

$$\tilde{\mathbf{v}}_i(t+\delta t) = \mathbf{v}_i(t) + \lambda \delta t \mathbf{f}_i(t),$$

$$\mathbf{f}_i(t+\delta t) = \mathbf{f}_i(\mathbf{r}(t+\delta t), \tilde{\mathbf{v}}(t+\delta t)),$$

$$\mathbf{v}_i(t+\delta t) = \mathbf{v}_i(t) + \frac{1}{2}\delta t[\mathbf{f}_i(t) + \mathbf{f}_i(t+\delta t)], \tag{13}$$

where $\mathbf{r}$, $\mathbf{v}$, and $\mathbf{f}$ denote the position, velocity, and force vectors, respectively, t denotes the time, i is a particle tag, and λ is an empirical parameter. The quantity $\tilde{\mathbf{v}}$ is a guessed value of the velocity. This guess is necessary because the force depends on velocity as seen from the third equation in (13).

III. RESULTS AND DISCUSSION

Some physical parameters useful in characterizing nanocylinder behavior will now be defined. Recall that, when the size of fluidic systems lies at the nanolevel, thermal fluctuations play an important role in determining the system behavior. These fluctuations arise because of the thermal energy possessed by atoms or molecules. Thermal fluctuations are manifested in the form of thermal capillary waves that are always present in the interfacial region. When the system size is large, the fluctuations do not influence the system behavior, but for small-sized systems they can play a dominant role. They can collectively lead to the generation of momentum imbalances which lead to capillary-induced breakup. That thermal fluctuations are captured by DPD has been shown in the literature [19,43], but its ability to predict nanocylinder breakup has not been assessed. To characterize the relative importance of thermally induced forces compared to capillary forces, a thermal length scale l_T can be defined as

$$l_T = \sqrt{\frac{k_BT}{\sigma_s}}, \tag{14}$$

where k_B denotes the Boltzmann constant, T the temperature, and σ_s the surface tension. The surface tension is determined by carrying out simulations of a liquid drop and deriving the surface tension from an application of Laplace law. This is initially derived for a reference temperature $k_BT=0.016$. The set of parameters for this simulation is kept the same as in nanocylinder breakup simulation. The following relation [44] based on mean-field theory is then used to calculate the surface tension at other temperatures:

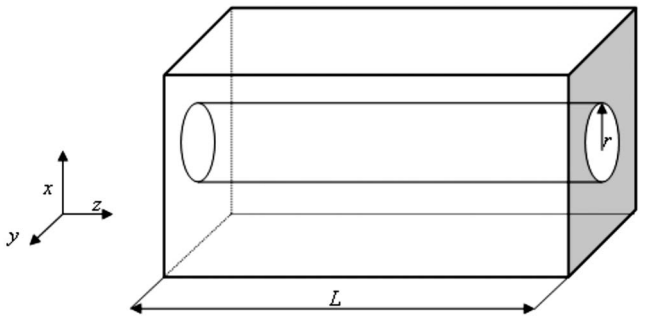

FIG. 1. Computational setup.

$$\sigma_s = \sigma_{so}\left(1 - \frac{T}{T_c}\right)^{1.5}. \tag{15}$$

The value of surface tension σ_s at $k_BT=0.016$ is determined to be 0.22 from the Laplace law. The mean-field critical temperature T_c for the simulated liquid is 0.0357 and σ_{so} is found to be 0.5366 from Eq. (15). The thermal length scale does not give much insight in absolute terms, but its importance can be assessed by examining a nondimensional length l^* defined as

$$l^* = \frac{L_c}{l_T}, \tag{16}$$

where L_c is a characteristic physical dimension. In this work, L_c is taken to be the radius of the cylinder. The value of l_T for typical liquids under standard conditions is of the order of a few nanometers. This implies that $l^* \sim O(1)$ for nanofluidic systems and, hence, shows the importance of thermal fluctuations for these systems.

The computational domain for the simulations is shown in Fig. 1. We apply periodic boundary conditions along the x, y, and z directions. The simulation parameters are given in Table I. The state point corresponding to these parameters gives a liquid-to-vapor density ratio of about 100. The initial configuration for all the simulations in this study is a uniform cubic arrangement of particles. The particles fill the computational domain to attain a liquid-vapor distribution corresponding to the simulated state point.

In the analysis and discussion, we will consider a nondimensional wave number given by

$$k = \frac{2\pi r}{\lambda}, \tag{17}$$

where λ is the wavelength of the disturbance. In our simulations the origin of the disturbance is thermal fluctuations. The maximum possible wavelength of this disturbance is equal to the axial length of the computational domain, i.e., in Eq. (17), λ is taken to be the length of the computational domain. When the length is much larger than the circumference of the cylinder, it is observed that multiple drops form, i.e., the length is sufficient to capture multiple modes of disturbance. If this happens, the wavelength of disturbance is taken as the length of the domain divided by the number of drops formed.

TABLE I. Simulation parameters.

Parameter	Equation in which the parameter appears	Value in DPD units
k_BT	(6), (12), (14)	1.6×10^{-2}
Mean-field critical temperature	(15)	3.57×10^{-2}
a (van der Waals parameter)	(9), (12)	3.012×10^{-3}
b (van der Waals parameter)	(9), (12)	2.5×10^{-2}
σ	(4), (6)	1.3×10^{-1}
κ	(8), (12)	1.0×10^{-3}
Time step δt	(13)	1.0×10^{-2}
r_c	(7), (11)	1.05

Figure 2 presents results, at different DPD times, from a simulation with the parameters in Table I. The number of DPD particles employed is 2880. The DPD time is computed as the DPD time step δt [see Eq. (13)] multiplied by the number of computational cycles completed. The simulations are performed with the value of $k=0.22$ based on the domain length, but the effective λ in Eq. (17) could be shorter. In fact, since two drops form in this case, k is effectively 0.44. The value of l^* in Eq. (16) is 3.52.

The disturbances present on the surface of the cylinder, as clearly evident in Fig. 2(c), grow with time and eventually lead to breakup as seen in Fig. 2(d). In this specific case, we see the formation of two drops which have different sizes. The drops have diameters larger than the cylinder diameter, as expected for capillary breakup. The quantitative ratio of the drop diameter to the cylinder diameter has not been estimated in this work because of the uncertainty in defining the surface of the sphere. Recall that this ratio is 1.89 for Rayleigh breakup [50]. The drop diameters visually appear greater than the diameter of the cylinder, but it is interesting to observe that the drops in the simulations are not of identical size. Nevertheless, there is no clear indication of satellite drops. After the breakup, the two drops attain velocities in opposite directions to conserve linear momentum; see Figs. 2(f) and 2(g). This leads to a merger of the drops as seen in Fig. 2(i). Note, however, that the simulations are stochastic; hence, the details of the process will not be repeated when a different random number seed is used.

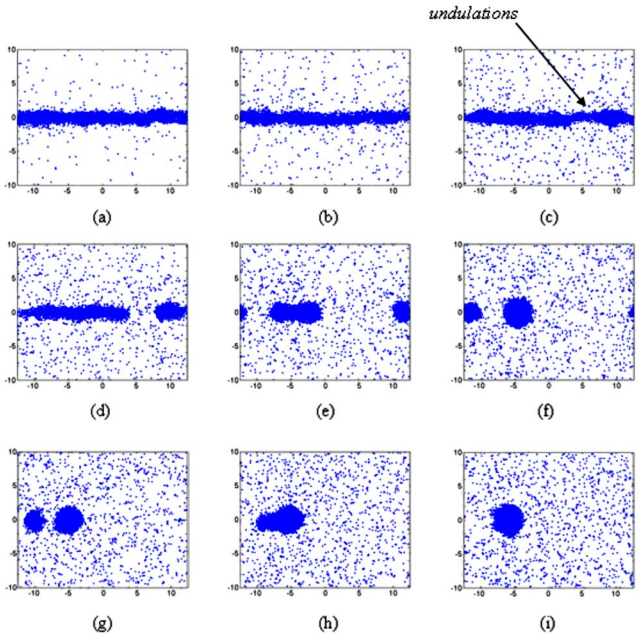

FIG. 2. (Color online) Snapshots of a liquid nanocylinder along the z-y plane at DPD times of (a) 50, (b) 100, (c) 150, (d) 200, (e) 250, (f) 300, (g) 350, (h) 400, and (i) 450; $k=0.22$ in Eq. (17).

Figure 3 shows results from a simulation at identical times as those in Fig. 2, but for a different seed. Notice that in this case also two drops are formed. The breaking occurs at approximately the same time as in Fig. 2. But one difference is that the drops do not merge. The details of the process are also somewhat dependent on the size of the domain. Figure 4 shows a set of results at identical times in a domain which has three times the size in the x and y directions, i.e., the length of the domain in the z direction is the same as in Fig. 2, but the width and depth are three times greater. The

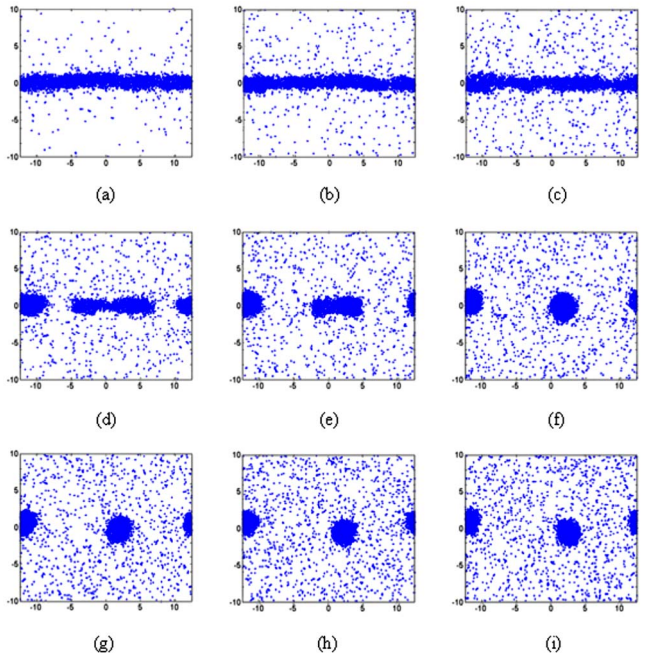

FIG. 3. (Color online) Snapshots of a liquid nanocylinder along the z-y plane at DPD times of (a) 50, (b) 100, (c) 150, (d) 200, (e) 250, (f) 300, (g) 350, (h) 400, and (i) 450; effect of random number seed.

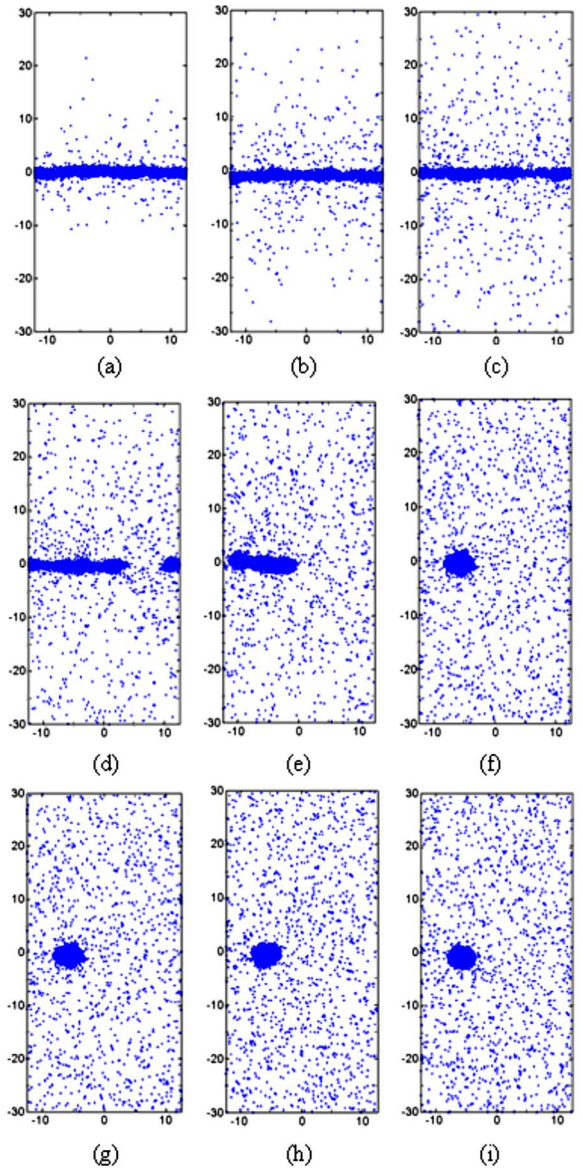

FIG. 4. (Color online) Snapshots of a liquid nanocylinder along the *z*-*y* plane at DPD times of (a) 50, (b) 100, (c) 150, (d) 200, (e) 250, (f) 300, (g) 350, (h) 400, and (i) 450; effect of domain size.

random seed was the same. The cylinder diameter is unchanged. The breakup occurs at about the same time as in the previous two cases, but only one drop is observed. Based on our earlier reasoning, in this case $k=0.22$ and not 0.44. A possible factor influencing the process is that, during the course of the simulations, the volume that lies outside the cylinder fills up with DPD particles as a result of vaporization. Hence, the density ratio is time dependent, and different for the two cases. This may have some influence, but the effects have not been quantified. In the case of capillary breakup of liquid cylinders at the macroscale, it is known that the breakup time will increase as k increases [51]; the relevant equations will be given later.

Next, simulations are carried out in a domain whose length (z direction) is increased by four times, but the radius of the cylinder is unchanged. The width and depth are the same as in Fig. 2. Hence, k in Eq. (17) decreases. It is expected that, since the results presented in Fig. 2 showed two drops, eight drops may form in this case. The results are presented in Fig. 5 at different times. Figures 5(e) and 5(f) are shown magnified to illustrate the details of the breakup process. The long thread breaks up into multiple drops as shown in Figs. 5(g)–5(j). This shows that the length of the computational domain is sufficient to capture multiple wavelengths. Seven drops are clearly observed, though it is possible that two of the drops may have combined [see Figs. 5(h) and 5(i)]. The breakup characteristics observed here are similar to those when the smaller domain was employed. Hence, the conclusions drawn there apply. At the point of breakup, long necks do not form; instead, double-cone structures are observed. This structure has been observed in the molecular dynamics simulations of nanojets performed by Moseler and Landman [7]. The liquid in the region joining the two cones gets drained and this, combined with the presence of thermal fluctuations, leads to the breakup that follows. In particular, notice that the drops are of approximately the same diameter, and somewhat larger than the cylinder diameter, as pointed out earlier.

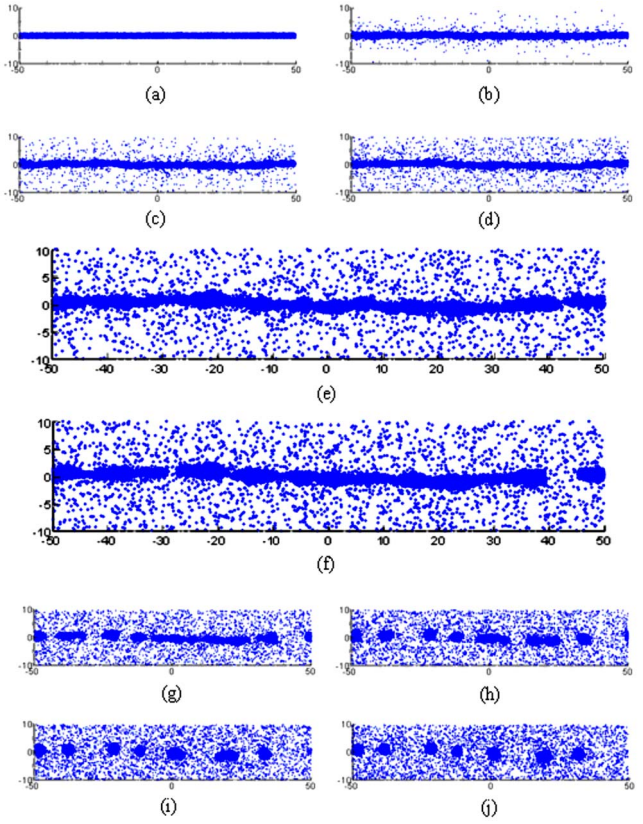

FIG. 5. (Color online) Snapshots of breakup of a liquid nanocylinder along the *z*-*y* plane at DPD times of (a) 1, (b) 30, (c) 60, (d) 90, (e) 120, (f) 150, (g) 180, (h) 210, (i) 240, and (j) 270; simulation with the cylinder length four times larger than in simulation in Fig. 2.

If Rayleigh's criterion holds, then breakup should not occur for values of k greater than 1. Consider Fig. 6, which presents snapshots of a liquid cylinder at different times when $k=1.26$. Three views of the computational domain

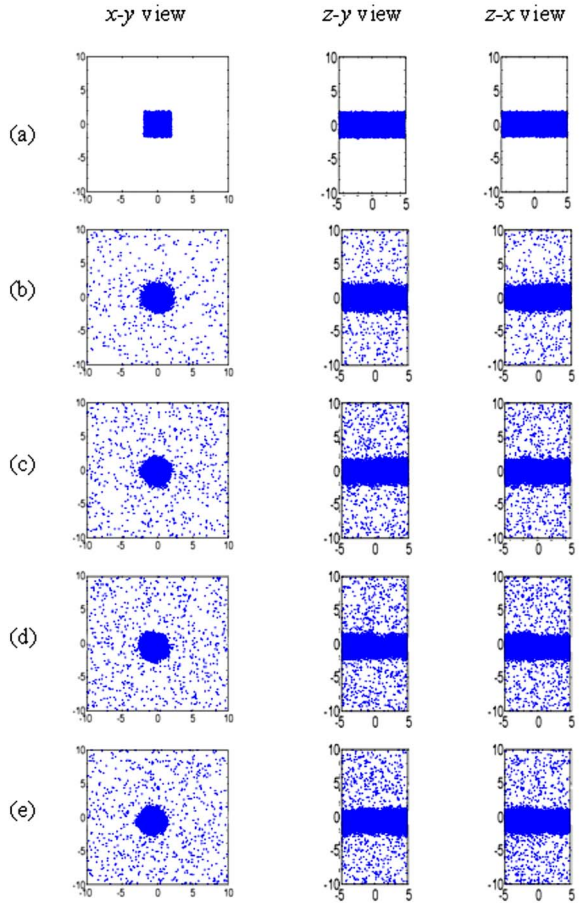

FIG. 6. (Color online) Snapshots of a nanocylinder with $k=1.26$ at DPD times of (a) 1, (b) 250, (c) 500, (d) 750, and (e) 1000.

along the x-y, z-y, and z-x directions are shown at DPD times of 1, 250, 500, 750, and 1000. As in the previous two cases, $l^*=3.52$. It is seen that the cylinder tends to remain stable with time and does not break up into drops though surface perturbations may be observed as a result of thermal fluctuations. A simulation performed at a higher value of $k=1.55$, i.e., by considering an even shorter domain, did not lead to breakup, adding credence to the applicability of the Rayleigh criterion. Of course, computations have to be carried out for

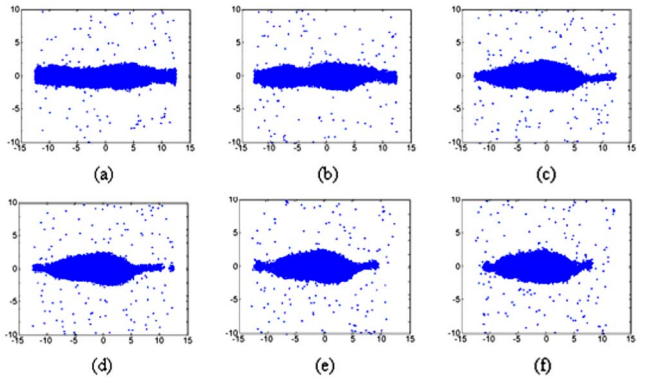

FIG. 7. (Color online) Snapshots of a liquid nanocylinder in periodic domain at DPD times of (a) 600, (b) 700, (c) 800, (d) 830 (e) 840, and (f) 850; $k_BT=0.01$.

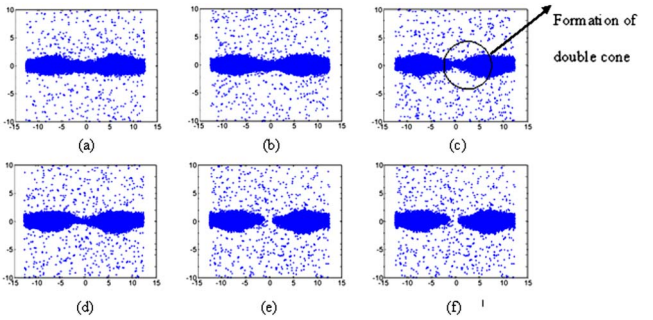

FIG. 8. (Color online) Snapshots of a liquid nanocylinder in periodic domain at DPD times of (a) 400, (b) 450, (c) 500, (d) 520, (e) 530, and (f) 540; $k_BT=0.013$.

a broad range of values of k to confirm if the transition point is indeed 1, but the general behavior is consistent.

It is interesting to observe the influence of changing the thermal length scale on the breakup process. This may be done by changing the temperature. Recall the definition of thermal length scale in Eq. (14). Figures 7–10 show the results for k_BT values of 0.01, 0.013, 0.016, and 0.019, respectively. The value of k in Eq. (17) is 0.47 in all cases. The values of l_T for the four cases are 0.175, 0.219, 0.270, and 0.333, respectively, and those of l^* are 8.016, 6.405, 5.191, and 4.209, respectively. Notice that the plots are shown at the point of breakup. When the thermal fluctuations are amplified by increasing the temperature, i.e., l^* decreases, we find that the breakup process is accelerated. The breakup times for the four cases are 840, 530, 460, and 290, respectively. In Fig. 8, the characteristic double-cone structure formed prior to breakup is highlighted. Several additional computations were carried out at different temperatures, and the breakup time as a function of k_BT is shown in Fig. 11. In general, there is a decrease in the breakup time with increasing temperature. Some of the variability in the figure may be attributed to the stochastic nature of the calculations. Another way to change the relative importance of the thermal length scales is to change the cylinder radius, i.e., L_c and hence l^* in Eq. (16) will change. Figure 12 shows the breakup time as a function of cylinder radius. It can be seen that as the radius increases, i.e., l^* increases, the time for breakup increases.

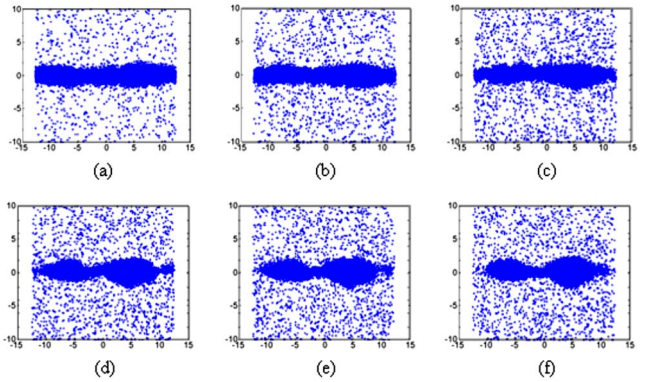

FIG. 9. (Color online) Snapshots of a liquid nanocylinder in periodic domain at DPD times of (a) 200, (b) 300, (c) 400, (d) 450, (e) 460, and (f) 470; $k_BT=0.016$.

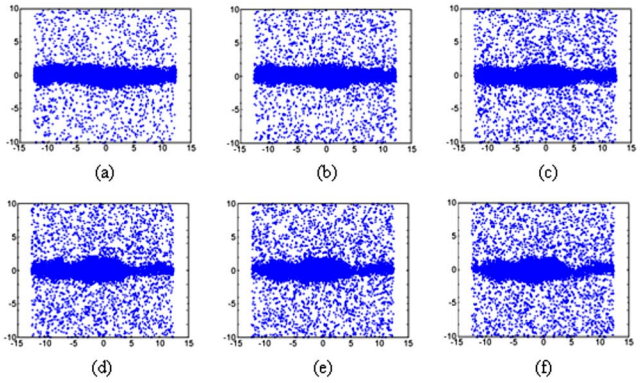

FIG. 10. (Color online) Snapshots of a liquid nanocylinder in periodic domain at DPD times of (a) 150, (b) 200, (c) 250, (d) 280, (e) 290, and (f) 300; $k_BT=0.019$.

Of course, it is possible that this is a reflection of increasing value of k which, as will be discussed later, will show increasing breakup time irrespective of the source of the disturbance.

In the case of breakup of macroscopic liquid cylinders, the formation of elongated threadlike structures has been reported for viscous liquids [6,52]. A characteristic length scale that gives the relative importance of viscous forces relative to the surface tension forces is the viscous length scale l_μ given by

$$l_\mu = \frac{\mu^2}{\rho\sigma_s}, \tag{18}$$

where μ is the dynamic viscosity, ρ is the density, and σ_s is the surface tension. It has been shown [6,52] that fluids with low viscosities have a cap-cone structure before breakup as compared to the long thin thread structures for fluids with high viscosities. To investigate the influence of increased viscosity on breakup behavior, a simulation was carried out in which the value of l_μ appearing in Eq. (18) is increased from 1.32 to 33.6. The results for the two compared cases are

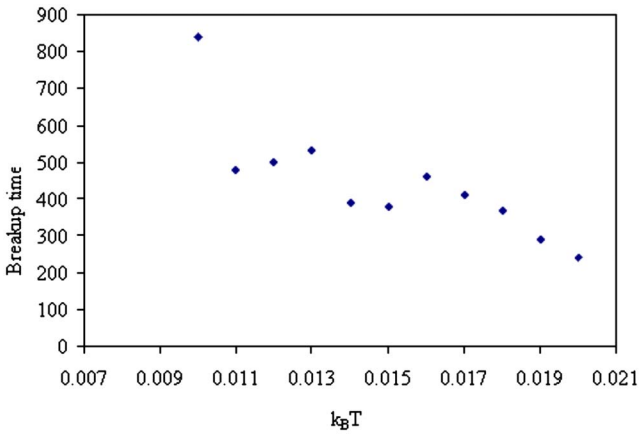

FIG. 11. (Color online) Variation of breakup time with system temperature k_BT.

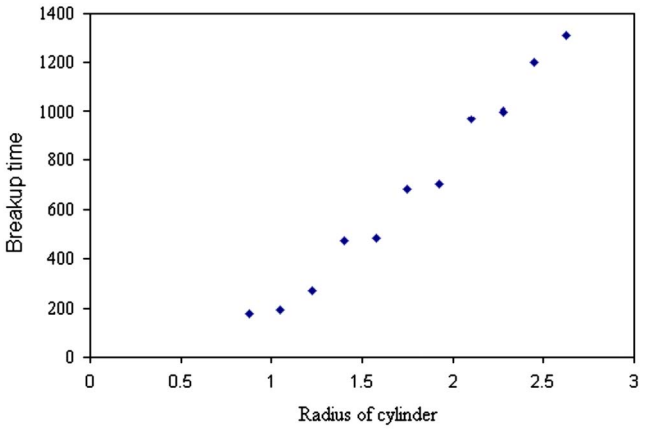

FIG. 12. (Color online) Variation of breakup time with cylinder radius.

presented in Figs. 5 ($l_\mu=1.32$) and 13 ($l_\mu=33.6$), respectively. The corresponding Ohnesorge number Oh, which is a measure of the relative importance of the viscous and surface tension forces, for the two cases is 0.836 and 4.216, respectively. Oh is defined as

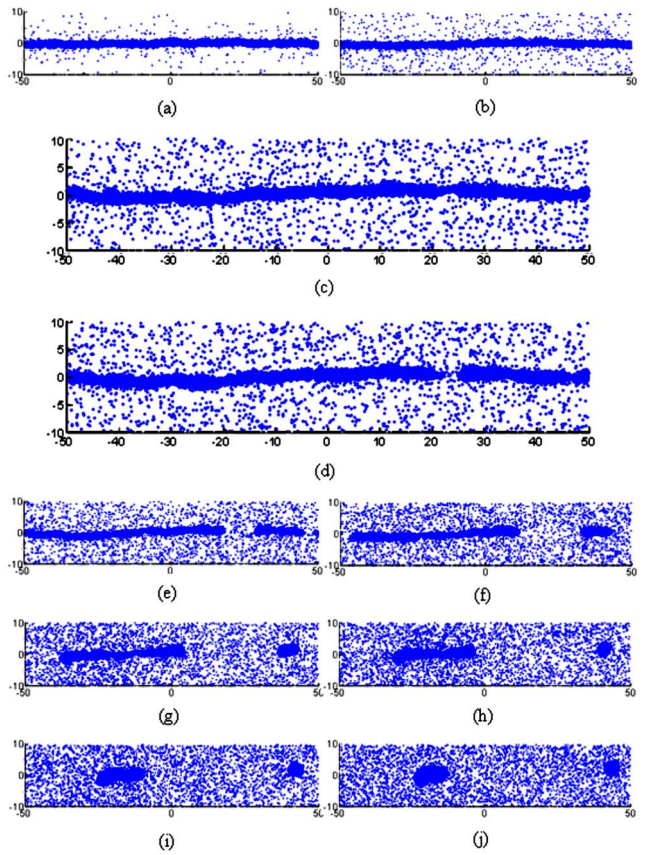

FIG. 13. (Color online) Snapshots of breakup of liquid nanocylinder along the z-x plane at DPD times of (a) 50, (b) 100, (c) 200, (d) 230, (e) 300, (f) 400, (g) 500, (h) 600, (i) 700, and (j) 800. Viscous length scale is about 25 times the value for simulation in Fig. 5.

TABLE II. Cases simulated for breakup of liquid nanocylinders.

Case no.	r	k	T_b	k_BT	N	C_1	C_2
1	0.875	0.2215	175	0.016	2880	2.66	13.51
2	1.050	0.266	191	0.016	3920	2.62	12.01
3	1.225	0.31	270	0.016	5120	3.37	14.16
4	1.400	0.354	475	0.016	6480	5.44	21.08
5	1.575	0.399	485	0.016	8000	5.13	18.34
6	1.750	0.443	682	0.016	9680	6.67	22.25
7	1.925	0.487	701	0.016	11520	6.35	19.73
8	2.100	0.531	970	0.016	13520	8.13	23.56
9	2.275	0.575	1000	0.016	15680	7.76	20.90
10	2.450	0.619	1200	0.016	18000	8.58	21.47
11	2.625	0.663	1310	0.016	20480	8.59	19.88
12	1.400	0.354	840	0.010	6480	11.74	55.57
13	1.400	0.354	480	0.011	6480	6.51	29.91
14	1.400	0.354	500	0.012	6480	6.58	29.28
15	1.400	0.354	530	0.013	6480	6.75	29.10
16	1.400	0.354	390	0.014	6480	4.80	20.01
17	1.400	0.354	380	0.015	6480	4.51	18.17
18	1.400	0.354	410	0.017	6480	4.51	16.83
19	1.400	0.354	370	0.018	6480	3.91	13.99
20	1.400	0.354	290	0.019	6480	2.93	10.04
21	1.400	0.354	240	0.020	6480	2.32	7.57

$$\mathrm{Oh} = \left(\frac{\mu_l}{\sqrt{\rho_l \sigma_s r}}\right), \tag{19}$$

where μ_l is the liquid dynamic viscosity, ρ_l is the liquid density, σ_s is the surface tension, and r is the radius of the nanocylinder. The viscosity is changed by changing the value of the amplitude γ appearing in the expression for the dissipative force [see Eq. (4)]. The simulation temperature is $k_BT=0.016$. Surface undulations are evident; but, unlike in macroscale cylinders, the formation of elongated threadlike structures is not seen, even at this higher viscosity. The breakup is seen to take place in Fig. 13(d). The DPD time at which the breakup occurs is about 230 in Fig. 13 compared to about 120 in Fig. 5. Hence, increasing the viscosity increases breakup time. A simulation was also carried out with a viscosity that was an order of magnitude greater than the higher value above, and no breakup was then observed. It is worth pointing out that according to Weber [53] the optimum wavelength for breakup will increase with viscosity. As the wavelength increases, the drop size will increase. The results presented are consistent with this theory. Notice that only two drops are observed in Fig. 13 whereas seven were observed in Fig. 5. Since the volumes of the initial cylinders were identical, this implies that drops are larger. This can be observed visually.

From scaling arguments, it is possible to derive the following relationships for the breakup time T_b of a cylinder due to capillary instabilities [51]:

$$T_b = C_1 \sqrt{\frac{r^3 \rho_l}{\sigma_s} \frac{I_0(k)}{I_1(k)} \frac{1}{k(1-k^2)}}, \tag{20}$$

$$T_b = C_2 \left(\frac{r\mu_l}{\sigma_s} \frac{1}{(1-k^2)}\right), \tag{21}$$

where μ_l is the dynamic viscosity, ρ_l is the density, σ_s is the surface tension, r is the radius of the cylinder, k is the nondimensional wave number, and I_0 and I_1 are modified Bessel functions. Equation (20) is applicable when viscosity is neglected, and Eq. (21) when viscosity is included, for capillary breakup of liquid cylinders at the macroscale. A series of simulations where ρ_l, σ_s, and μ_l were varied were carried out. If, for the range of computations, it can be shown that constant values of C_1 or C_2 can be obtained, then the implication is that either Eq. (20) or Eq. (21) is applicable for nanocylinders.

Table II shows the results for several cases. The values of C_1 and C_2 derived for each case are also shown. Notice that constant values of C_1 and C_2 are not obtained. The average value of C_1 is 5.71 ± 2.43, whereas that of C_2 is 20.83 ± 9.97. Notice from Table II that if only the first 11 cases, i.e., when k_BT is a constant and only r varies, are considered then the values of C_2 show less variation. In fact, in this case the average values of C_1 and C_2 are 5.94 ± 2.29 and 18.81 ± 3.86. So the greater variability arises when k_BT changes for cases 12–21. A change in k_BT results in a change in μ_l and σ_s, and in the thermal length scale l_T. Recall that the thermal length scale is a measure of thermally induced fluctuations at the liquid surface. It is possible that the change in l_T may lead to different relations at the nanolevel than the ones given by Eqs. (20) and (21). Consider the following relation from linear instability theory [36,51]:

$$\eta = \varepsilon e^{\xi t}, \tag{22}$$

where η is the displacement of the interface, ε is the amplitude of the disturbance, ξ is the growth rate, and t is the time. For thermally induced breakup, ε is a function of the temperature of the system and, say, is proportional to the thermal length scale l_T. Note that this is an assumption. While it can be stated with some confidence that the origin of the disturbance at the nanolevel is the thermal fluctuation, it is not clear that the amplitude of the disturbance is proportional to l_T. For example, it has been suggested that the fluctuations which lead to breakup at the nanolevel do not directly result from thermal fluctuations, but indirectly from momentum imbalance induced by thermal fluctuations. Nevertheless, if this line of reasoning is pursued,

$$\eta \propto l_T e^{\xi t} \tag{23}$$

or

$$\eta = C_3 l_T e^{\xi t}, \tag{24}$$

i.e.,

$$\ln\left(\frac{\eta}{C_3 l_T}\right) = \xi t, \tag{25}$$

where C_3 is a constant. For a fixed temperature, the thermal length scale l_T is a constant. Then at the breakup point

$$\ln\left(\frac{\eta_1}{C_3 l_T}\right) = \xi T_b = \chi, \tag{26}$$

where η_1 is the displacement of the interface at the time of breakup. The variable χ is a function of temperature and, as the temperature increases, l_T will increase. This implies that χ will decrease with increasing temperature. In deriving Eqs. (20) and (21), it is assumed that χ is a constant. Unfortunately, further analysis that has been carried out to see if the data of Table II are consistent with Eq. (26) is inconclusive (and, hence not presented), but the discussion above points to the possibility that Eqs. (20) and (21) derived for macroscale considerations may not be applicable at the nanoscale. It is interesting to recall that results were presented earlier (compare Figs. 5 and 13) where the viscosity was increased by changing the value of γ in Eq. (4), and not by changing temperature. A factor-of-5 increase in viscosity changed the breakup time from 120 to 230 in that case. Again, the results do not scale with Eq. (21), since according to this equation the breakup should have increased by 4.31 times, taking into account the change in viscosity and k. This suggests that the lack of conformity with Eq. (21) is not just related to changes in temperature. DPD has not been employed for simulation of liquid nanocylinders in the past, and it is possible that the difference in behavior highlighted above arises from a shortcoming of the method itself. Computations with MD can clarify this.

The transient behavior of the minimum radius $r_{\min}$ where breakup occurs will now be examined. Macroscopic theory predicts the relationship for $r_{\min}$ given in Eq. (1). As shown by Eggers [27], there is an acceleration of the reduction of the radius at the nanolevel. The corresponding relation is given by Eq. (2). In the simulations performed in this study the characteristic length $l^* \sim O(1-10)$. It has also been shown that symmetric double-cone structures form prior to the breakup. So it is expected that the form of $r_{\min}$ given by Eq. (2) will be recovered from the simulations. Figure 14 presents the results for $r_{\min}$ as a function of $(T_b - t)$ for one of the simulations. The parameter r_1 in Eq. (2) is determined by a least-squares fit to the DPD data. It can be seen that the variation in $r_{\min}$ from DPD simulations follows the trend from Eq. (2).

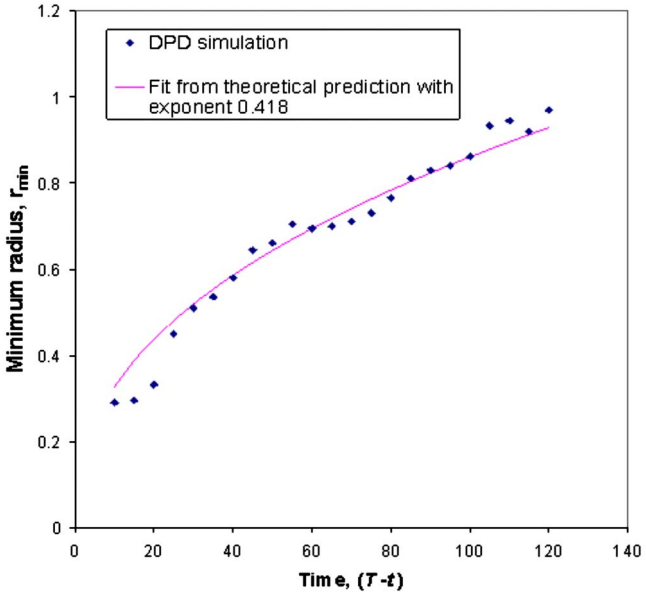

FIG. 14. (Color online) Minimum cylinder radius $r_{\min}$ as a function of time $(T_b - t)$. Note that T_b is the breakup time.

IV. SUMMARY AND CONCLUSIONS

In this work, a DPD-based model for two-phase flows is employed to simulate the breakup of liquid nanocylinders. It is shown that the model is able to capture the thermally induced breakup of the cylinders. The results are in agreement with prior theoretical and molecular dynamics simulation results. These results will now be summarized. It is shown that Rayleigh's stability criterion, which states that liquid cylinders are unstable to disturbances with wavelengths greater than their circumference, applies for the simulations carried out in this study. This is in agreement with prior MD simulations. Also in agreement with prior MD simulations, the formation of satellite drops is not observed. This has been attributed to the dominant role of thermal fluctuations at the nanolevel. These fluctuations cause a symmetric breakup of the liquid neck with a double-cone structure that precludes the formation of satellite drops as pointed out in prior work. This has important implications from a practical point of view as the satellite drops, owing to their smaller size, behave differently and require special attention in applications like ink-jet printing. Their nonoccurrence at the nanolevel leads to uniform distribution of drop sizes. It is also shown that thermal fluctuations accelerate the breakup

dynamics near the breakup point, the results of which are in agreement with theoretical predictions by Eggers [25]. In agreement with prior MD studies, it is shown that, as the radius of the cylinder increases, the change in breakup time is consistent with macroscale relationships. However, in additional simulations, it is shown that the breakup time does not scale with the macroscale relationships when liquid viscosity and surface tension are varied. As indicated in the text, it is possible that this may result from limitations of the DPD model. Nevertheless, the fact that DPD results are in agreement with prior MD simulations and theoretical predictions, when such results and predictions are available, suggests that the conclusions about breakup time may be correct. Computations with MD can confirm this.

[1] Y. Y. Ye, R. Biswas, J. R. Morris, A. Bastawros, and A. Chandra, Nanotechnology **14**, 390 (2003).
[2] K. Murata, J. Matsumoto, A. Tezuka, Y. Matsuba, and H. Yokoyama, Microsyst. Technol. **12**, 2 (2005).
[3] D. Cuvelier, I. Derenyi, P. Bassereau, and P. Nassoy, Biophys. J. **88**, 2714 (2005).
[4] I. Shiyanovskaya, K. D. Singer, V. Percec, T. K. Bera, Y. Miura, and M. Glodde, Phys. Rev. B **67**, 035204 (2003).
[5] P. A. Furth, Mol. Biotechnol. **7**, 139 (1997).
[6] J. Eggers, Rev. Mod. Phys. **69**, 865 (1997).
[7] M. Moseler and U. Landman, Science **289**, 1165 (2000).
[8] G. De Fabritiis, M. Serrano, R. Delgado-Buscalioni, and P. V. Coveney, Phys. Rev. E **75**, 026307 (2007).
[9] M. P. Allen, *Computer Simulation of Liquids* (Oxford Science Publications, Oxford, 1987).
[10] J. Koplik and J. R. Banavar, Annu. Rev. Fluid Mech. **27**, 257 (1995).
[11] D. R. Heine, G. S. Grest, and E. B. Webb III, Phys. Rev. E **68**, 061603 (2003).
[12] Y. S. Choi, S. J. Kim, and M.-U. Kim, Phys. Rev. E **73**, 016309 (2006).
[13] H. Shin, M. Oschwald, M. M. Micci, and W. Yoon, Nanotechnology **16**, 2838 (2005).
[14] M. Cieplak, J. Koplik, and J. R. Banavar, Phys. Rev. Lett. **86**, 803 (2001).
[15] J. Koplik and J. R. Banavar, Phys. Rev. Lett. **96**, 044505 (2006).
[16] K. Kadau, T. C. Germann, N. G. Hadjiconstantinou, P. S. Lomdahl, G. Dimonte, B. L. Holian, and B. J. Alder, Proc. Natl. Acad. Sci. U.S.A. **101**, 5851 (2004).
[17] E. E. Keaveny, I. V. Pivkin, M. Maxey, and G. E. Karniadakis, J. Chem. Phys. **123**, 104107 (2005).
[18] V. Symeonidis, G. E. Karniadakis, and B. Caswell, Phys. Rev. Lett. **95**, 076001 (2005).
[19] P. J. Hoogerbrugge and J. M. V. A. Koelman, Europhys. Lett. **19**, 155 (1992).
[20] P. Espanol and P. Warren, Europhys. Lett. **30**, 191 (1995).
[21] S. Chen and G. D. Doolen, Annu. Rev. Fluid Mech. **30**, 329 (1998).
[22] S. Succi, *The Lattice Boltzmann Equations for Fluid Dynamics and Beyond* (Oxford University Press, Oxford, 2001).
[23] M. E. McCracken and J. Abraham, Phys. Rev. E **71**, 036701 (2005).
[24] K. N. Premnath and J. Abraham, Phys. Rev. E **71**, 056706 (2005).
[25] J. Eggers, Phys. Rev. Lett. **89**, 084502 (2002).
[26] E. S. Boek, P. V. Coveney, H. N. W. Lekkerkerker, and P. van der Schoot, Phys. Rev. E **55**, 3124 (1997).
[27] X. Fan, N.-P. Thien, N. T. Yong, X. Wu, and D. Xu, Phys. Fluids **15**, 11 (2003).
[28] P. De Palma, P. Valentini, and M. Napolitano, Phys. Fluids **18**, 027103 (2006).
[29] I. Pagonabarraga and D. Frenkel, J. Chem. Phys. **115**, 5015 (2001).
[30] P. B. Warren, Phys. Rev. E **68**, 066702 (2003).
[31] M. Liu, P. Meakin, and H. Huang, Phys. Fluids **18**, 017101 (2006).
[32] A. Tiwari and J. Abraham, Phys. Rev. E **74**, 056701 (2006).
[33] J. Koplik and J. R. Banavar, Phys. Fluids A **5**, 521 (1993).
[34] L. Rayleigh, Philos. Mag. **34**, 145 (1892).
[35] D. Min and H. Wong, Phys. Fluids **18**, 024103 (2006).
[36] S. Kawano, Phys. Rev. E **58**, 4468 (1998).
[37] D. Rutland and G. Jameson, J. Fluid Mech. **46**, 267 (1971).
[38] P. Lafrance, Phys. Fluids **18**, 428 (1975).
[39] A. Tiwari and J. Abraham, Microfluid. Nanofluid. **4**, 227 (2008).
[40] W. Kang and U. Landman, Phys. Rev. Lett. **98**, 064504 (2007).
[41] J. R. Lister and A. S. Stone, Phys. Fluids **10**, 2758 (1998).
[42] O. A. Basaran, AIChE J. **48**, 1842 (2002).
[43] R. D. Groot and P. B. Warren, J. Chem. Phys. **107**, 4423 (1997).
[44] J. Rowlinson and B. Widom, *Molecular Theory of Capillarity* (Clarendon Press, Oxford, 1982).
[45] D. Chandler, J. Weeks, and H. Anderson, Science **220**, 787 (1983).
[46] X. He, S. Chen, and R. Zhang, J. Comput. Phys. **152**, 642 (1999).
[47] L. B. Lucy, Astron. J. **82**, 1013 (1977).
[48] O. Kum, W. G. Hoover, and C. G. Hoover, Phys. Rev. E **68**, 017701 (2003).
[49] W. G. Hoover and C. G. Hoover, Phys. Rev. E **73**, 016702 (2006).
[50] Lord Rayleigh, Proc. London Math. Soc. **10**, 4 (1878).
[51] S. Chandrasekhar, *Hydrodynamic and Hydromagnetic Stability* (Clarendon Press, Oxford, 1961).
[52] X. D. Shi, M. Brenner, and S. R. Nagel, Science **265**, 219 (1994).
[53] C. Weber, Z. Angew. Math. Mech. **11**, 136 (1931).